Material and structural behaviour of PMMA from low temperatures to over the glass transition: Quasi-static and dynamic loading

D. Garcia-Gonzalez, A. Rusinek, A. Bendarma, R. Bernier, M. Klosak, Slim Bahi

Version of Record: https://www.sciencedirect.com/science/article/pii/S0142941819318811
Manuscript_d66f5d09a9c27a87dac4e4800fe79f68

Material and structural behaviour of PMMA from low temperatures to over the glass transition: Quasi-static and dynamic loading

D. Garcia-Gonzalez[1], A. Rusinek[2,3], A. Bendarma[4], R. Bernier[2], M. Klosak[4], S. Bahi[2]

[1] *Department of Continuum Mechanics and Structural Analysis, University Carlos III of Madrid, Avda. de la Universidad 30, E-28911 Leganés, Madrid, Spain*

[2] *Laboratory of Microstructure Studies and Mechanics of Materials, UMR-CNRS 7239, Lorraine University, 7 rue Félix Savart, BP 15082, 57073 Metz Cedex 03, France*

[3] *Chair of Excellence, Departamento de Ingeniería Mecánica, UC3M (Universidad Carlos III de Madrid) Avda. de la Universidad 30, 28911 Leganés, Madrid, España*

[4] *Laboratoire d'Innovation Durable et de Recherche Appliquée (L.I.D.R.A), Universiapolis, Bab Al Madina, Qr Tilila, Agadir, Morocco*

Abstract: This work aims at characterizing the mechanical behaviour of polymethyl-methacrylate (PMMA) under high velocity impact conditions over a wide range of testing temperatures. To this end, the mechanical response at uniaxial compression is studied for both quasi-static and dynamic conditions covering testing temperatures below, at and above glass transition. A pseudo-brittle to ductile transition in the failure of PMMA is observed at a threshold that depends on testing temperature and strain rate. This analysis allows for the interpretation of the perforation impact tests and to explain the principal deformation and failure mechanisms. To complete the study, the Richeton model to predict yielding is revisited. Finally, we provide a new constitutive model for finite deformations to further identify the deformation mechanisms governing the mechanical behaviour of PMMA and the influence of temperature and strain rate on them.

Keywords: PMMA; Impact behaviour; Polymer; Constitutive modelling; Glass transition

1. Introduction

Thermoplastic polymers have received both scientific and industrial interest due to their low density, relatively low cost and their suitability to replace metals in many technical applications [1,2]. During the last decade, this interest has become even more evident due to the development of new manufacturing techniques based on 3D printing [3]. In this regard, thermoplastic polymers allow for their manufacturing by fused deposition modelling (FDM) enabling customizable components and rapid prototyping [4]. Moreover, some applications still require traditional manufacturing (e.g., injection moulding) when they need to provide structural support or may be subjected to dynamic loading, such as in aeronautical, automotive or biomedical applications [5-9]. In this regard, thermoplastic polymers such as poly-ether-ether-ketone (PEEK), polyethylene or polymethyl-methacrylate (PMMA) are common solutions for the manufacturing of the aforementioned components. In particular, PMMA highlights for its strength and transparency and is widely used in automotive and aeronautical applications [10]. The mechanical behaviour of these polymers is rather complex since they present nonlinear response, strain rate, stress state and temperature dependencies as well as behaviour transitions associated to thermal-activated processes occurring within their microstructure [11-15]. In addition, their mechanical behaviour becomes even more complex under dynamic conditions where inelastic dissipation takes place resulting in adiabatic heating and subsequent thermal softening [16-19]. These effects are of extreme relevance when dealing with impact or perforation loading. In such situations,

local deformations lead to thermal and permanent deformation gradients resulting in microstructural changes associated to polymeric chains mobility and arrangement [20]. These microstructural changes thus lead to different macroscopic deformation and failure mechanisms. In this regard, Garcia-Gonzalez and co-authors [21,22] analysed the mechanical behaviour of PEEK and PEEK composites under impact conditions. Moreover, Mohagheghian et al. [23] performed perforation tests on polyethylene specimens. In this investigation, an identification of the relationship between the projectile tip geometry and impact energy absorption of polyethylene thermoplastics is done. Although different failure mechanisms were observed depending on the projectile nose (i.e., blunt, hemi-spherical, conical), a ductile behaviour was identified for all tests. However, ductile-to-brittle fracture has been observed for thermoplastic polymers subjected to impact loading depending on the testing temperature [24]. Regarding PMMA, the glass transition is estimated close to $T_g = 105°C$ as reported in Ref. [19]. The transition α corresponds to a strong dumping effect of the material close to T_g followed by a fast decrease of the storage modulus.

To further understand and explain the deformation mechanisms governing the mechanical response of thermoplastic polymers, several authors have proposed constitutive models describing the deformation process of these polymers. These models can be classified into two main groups: purely phenomenological models and physically motivated models. The former models aim at proposing mathematical equations to fit the mechanical response of these polymers. They usually incorporate specific functions to capture the dependences of, for example, yield stress on temperature or strain rate. Among them, for its relevance and impact on the state of the art, the model proposed by Richeton et al. [17, 25] is highlighted. This model proposes a set of mathematical expressions to define the yield stress of PMMA depending on temperature and strain rate along the glass transition of this material. On the other hand, several authors have developed constitutive models that are physically motivated and allow for the mechanical description of thermoplastic polymers. These models are usually based on the arrangement of rheological elements and hyperelastic energy potentials representing different deformation mechanisms. In this regard, Boyce et al. [26] developed a model to describe the mechanical response of PMMA. Richeton et al. [25] extended their previous phenomenological approach to a finite deformation model for PMMA. Garcia-Gonzalez and co-authors [15,16,27], in a series of works, developed thermodynamically consistent models for thermoplastic materials accounting for strain rate, temperature and stress state dependencies as well as for temperature evolution due to inelastic dissipation and thermal transitions in the response of the material.

Although the mechanical behaviour of thermoplastic polymers has been extensively studied, there is still a gap of knowledge in the effect of testing temperature on the impact and perforation behaviour of thermoplastic polymers at both low and high temperatures. Aiming at analysing the effect of temperature and the polymeric transitions associated, this work presents a complete study of the mechanical response of PMMA at high impact velocity covering testing temperatures from 20 ºC to 140 ºC. To better understand the deformation and failure mechanisms governing the perforation process, a first set of tests has been performed under uniaxial compression for both quasi-static and dynamic conditions and different initial temperatures. To complete the study, the model developed by Richeton et al. [17] has been revisited to predict yield stress. Finally, a new constitutive model is proposed to analyse the deformation mechanisms governing the mechanical behaviour of PMMA. This model is focused on the mechanical behaviour of PMMA above the glass transition. The model is developed for finite deformations and accounts for temperature and strain rate dependencies.

2. Experimental characterization under compression loading

This section characterises the mechanical behaviour of PMMA for quasi-static and dynamic loading at different initial temperatures (T_0) covering the three thermo-mechanical regions: glassy region (below glass transition); glass transition region; rubbery region (above glass transition). To this end, a screw machine has been used for quasi-static tests up to $10^{-1}\ s^{-1}$and a Split Hopkinson Pressure Bars (SHPB)

for dynamic conditions at high strain rates. The specimen used respects the ratio of $s_0 = H_0/\emptyset_0 \geq 0.5$ (corresponding to the initial height H_0 and diameter $\emptyset_0$ of the specimen) to avoid friction and inertial effects, as discussed in detail in Refs. [14, 28-31]. The tests at high temperatures are performed using the set-up described originally in Ref. [19]. At low temperature, a cryogenic gas is pulsed in a box fixed around the specimen allowing to reach a uniform temperature distribution. The temperature is monitored using a thermocouple linked to a controller. Depending on the target temperature, a cryogenic pump pulls the nitrogen gas inside the chamber when needed [33]. In all cases, a waiting time of 30 min has been used to reach uniform temperature within the specimen. These results are shown in Fig. 1. Note that the principal focus of this section is the analysis of transitions in the failure/deformation behaviour of PMMA. These material transitions are associated to free volume and mobility of polymeric chains, which are intimately related to temperature and strain rate. For lower strain rates, the failure transition is observed at lower temperatures, thus motivating the low testing temperatures chosen for these tests. Moreover, when increasing the strain rate, the failure transition moves to higher temperatures. Therefore, we selected a higher temperatures range for dynamic tests.

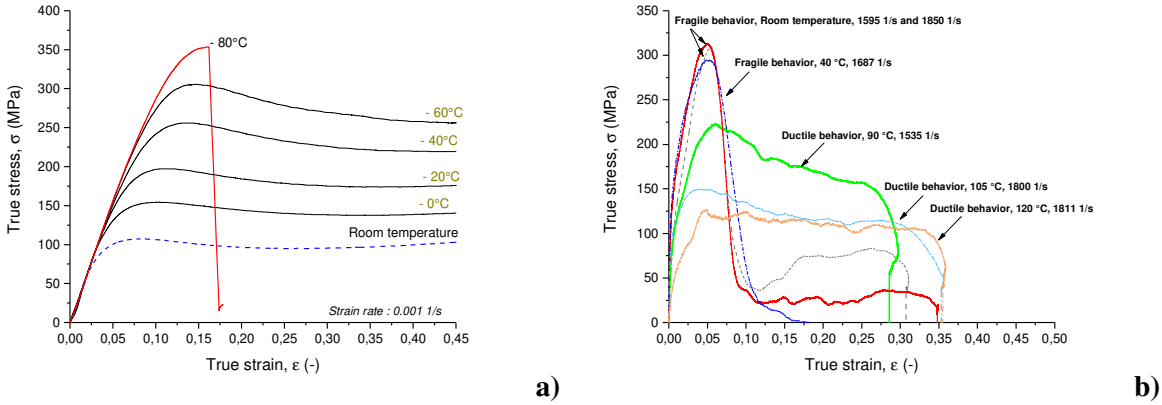

Fig. 1: Material behaviour description: a) Temperature effect under quasi-static loading; b) Temperature effect under dynamic loading.

From the quasi-static results (Fig. 1a), a pseudo-brittle to ductile transition is identified at a temperature threshold of $T_0 = -80$ ºC. At temperatures above the aforementioned threshold, a pseudo-brittle behaviour is observed presenting failure strain values around 15%. For testing temperatures above such threshold, a ductile behaviour is observed. The transition between ductile and pseudo-brittle response under quasi static loading is between $-80°C \leq T_0 \leq -60°C$. Moreover, a decrease in temperature also leads to higher yield stress σ_y. In this regard, a ratio close to $\frac{\sigma_y^{-60°C}}{\sigma_y^{T_{room}}} \sim 3.5$ is found when comparing the ratio of the yield stress between room temperature and the lowest temperature tested.

From the dynamic results, the pseudo-brittle to ductile transition is identified at a temperature threshold of $T_0 = 40°C$. At room temperature, a pseudo-brittle behaviour with a maximum strain level of failure close to $\varepsilon_{T_{room}}^{Dyn} \sim 0.07$ is observed. However, if the temperature increases above $T_0 = 40°C$, the material behaviour starts to behave in a ductile manner. This shift in the brittle to ductile transition with respect to quasi-static loading may be explained by the competition between the effects of temperature and strain rate on the polymeric chains mobility. In this regard, an increase in temperature favours chain mobility, thus resulting in an increase in ductility; whereas an increase in strain rate blocks the mobility of the chains. Concerning dynamic loading, the material at low and at room temperature is brittle, Fig. 1b.

A further dynamic characterisation has been performed at high temperatures, $T_0 \geq T_g$. This analysis aims at studying the mechanical behaviour of PMMA at the rubbery region when a ductile response is

expected. As reported for two strain rates, the hardening shape change for a temperature bigger than $T_0 \geq 120$ °C, see Fig. 2. Note that, to help interpretation and comparison of the results shown in Fig. 2, two reference strain rates have been used. The experimental strain rates showed less than 15% differences to the reference values. This response can be explained by a more relevant role of the polymeric network contribution to the overall stress response. This hypothesis is further discussed and interpreted with the help of a physically-motivated constitutive model in Section 5.

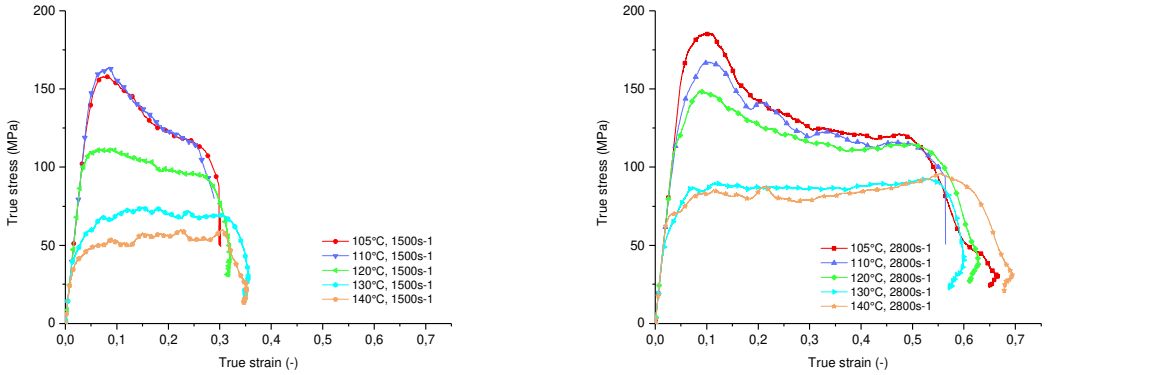

a) b)

Fig. 2: Material behaviour of PMMA for different initial temperatures; a- 1500 1/s; b- 2800 1/s.

From these results, it can be concluded that the energy required to induce failure increases with temperature and is associated with a strong increase in ductility. This observation is a key point to analyse the structure behaviour under impact and perforation as it will be discussed next.

3. Impact and perforation tests for different initial temperatures

In addition to the definition of the macroscopic behaviour of PMMA for a large range of strain rates and temperatures, a complete study has been performed under impact and perforation loading. Based on the previous results, that the PMMA is observed to behave ductile or fragile depending on the loading conditions (see Fig. 1). To this end, impact and perforation tests have been performed using a pneumatic gas gun coupled to a thermal chamber as described in Ref. [19]. The projectile shape is conical with a mass of $m_p = 28\ g$. The projectile nose angle is equal to $\phi_p = 36°$. When the plate is fixed in the furnace, a waiting time of 20 min is used to ensure uniform temperature distribution along the plate [19, 30, 32].

The results in terms of ballistic limit $V_B(T_0)$ depending on the initial temperature are reported in Fig. 3. Different slopes can be observed analysing the results by means of the V_B/T_0 ratio. In this regard, a slightly continuous increase is observed with testing temperature until around 80 ºC. Then, a sharp increase in ballistic limit occurs for temperatures from 80 ºC to 100 ºC. This change of tendency can be explained by a transition from quasi-brittle failure to ductile. Then, above the glass transition, the material undergoes a marked decrease in stiffness leading to a complete change in the V_B/T_0 trend, sharply decreasing the ballistic limit with testing temperature. For testing temperatures close to the glass transition, there is a strong competition by means of energy absorption capability between the thermal softening (reducing the energy absorption) and the increase in ductility (improving the energy absorption), see Fig. 3. Thus, from room temperature to glass transition ($T_g = 105°C$), the ballistic limit is twice bigger. For temperatures above glass transition, the ballistic limit is progressively reduced but still higher than the reference obtained at room temperature.

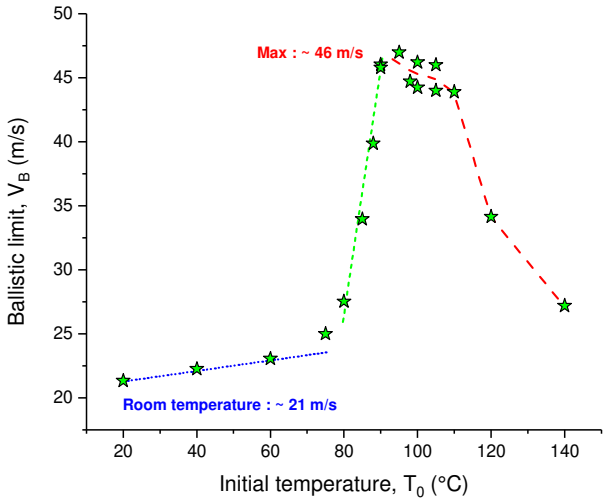

Fig. 3: Description of the ballistic limit depending on the initial temperature, transition from fragile to ductile.

The residual velocity V_R and absorbed energy W, depending on the impact velocity V_0, can be estimated for different initial temperatures T_0 using the Recht et al. description [34]:

$$V_R(T_0) = \left[{V_0}^{\alpha(T_0)} - {V_B}^{\alpha(T_0)}(T_0)\right]^{\frac{1}{\alpha(T_0)}} \quad (1)$$

$$W(T_0) = \frac{1}{2} \cdot m_P \cdot \left[{V_0}^2 - {V_R}^2(T_0)\right] \quad (2)$$

where $V_B(T_0)$ is the ballistic limit depending on the initial temperature (obtained from Fig. 3) and α is a fitting parameter proportional to the temperature as discussed in Ref. [34].

The predicted energy absorbed by Eq. (2) versus the impact velocity for different testing temperatures is compared with the experimental results in Fig. 4. This analytical approximation captures the trends from room temperature up to $T_0 = 90°C$. However, at and above glass transition, the model does not predict correctly the experimental values at high impact velocity $V_0 > 120\, m/s$. For these specific conditions, the plate cannot absorb a large quantity of energy.

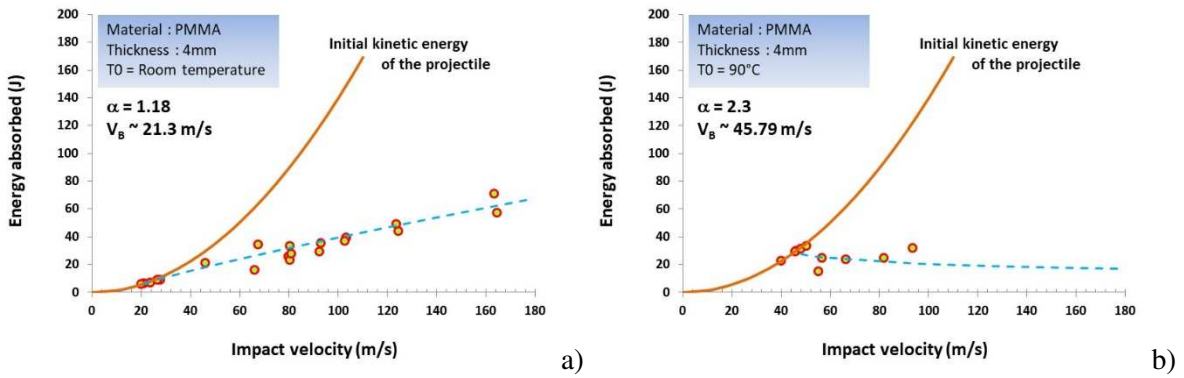

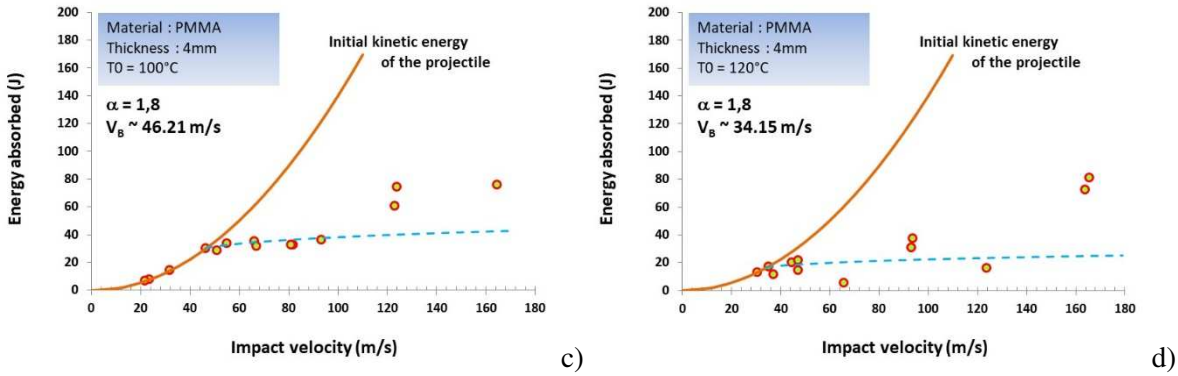

Fig. 4: Energy absorption for different initial temperatures, comparison between experiments and analytical model: a) Room temperature; b) 90°C; c) 100°C; d) 120°C

Next, an analysis by means of failure mode is performed. Fig. 5 reports the last stage of the perforation process at ballistic limit conditions depending on testing temperature. At temperatures lower than $T_0 < 90°C$, PMMA behaves in a brittle manner with cracks propagation inducing debris. For higher temperatures than $T_0 > 90°C$, the failure cracks propagation is limited and the failure mechanism changes to plug ejection showing a transition to a more ductile response. Finally, for temperatures above glass transition $T_0 > 100°C$, there is a clear transition to ductile behaviour where the PMMA behaves as a rubber like material. In such cases, the perforation induces a hole enlargement without showing cracks and, after complete perforation, there is a spring back mechanism resulting in the hole reclosing.

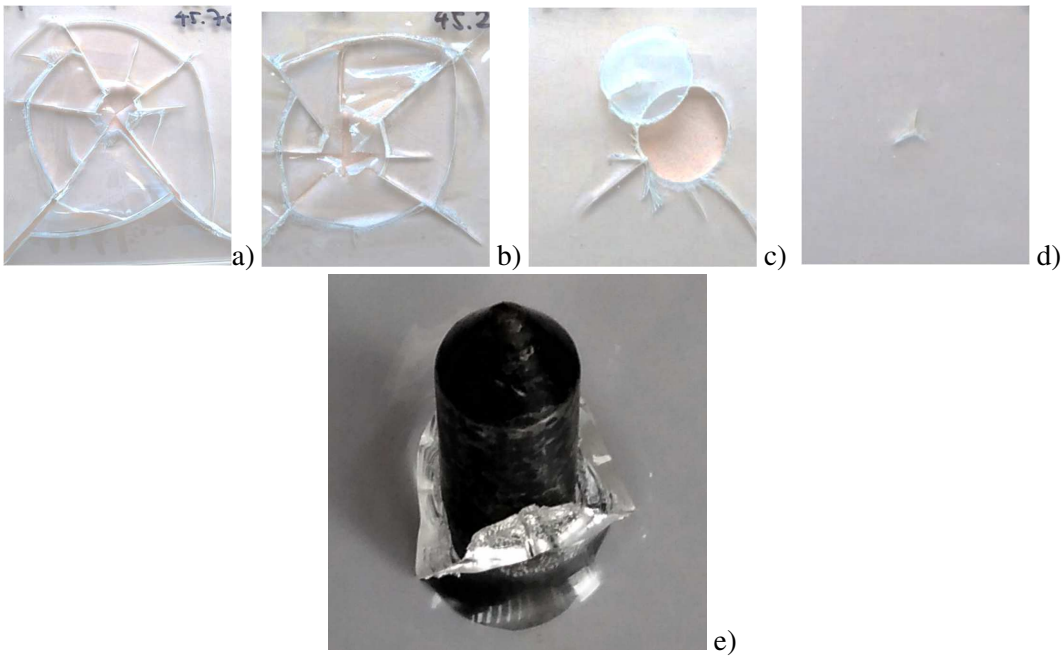

Fig. 5: Failure mode of PMMA for the ballistic limit at different temperatures: a) Room temperature; b) 60°C; c) 90°C; d) 105°C; e) 105°C and an initial velocity close to V_B.

Regarding this last case, Fig. 5d-e, for a testing temperature above glass transition, the kinematic of the perforation process can be described in 4 steps as proposed in Fig. 6. The first one corresponds to the impact of the projectile generating a small hole due to the projectile shape (conical) and some petals. Then, the projectile goes through the plate inducing a radial expansion of the initial hole until reaching

the dimension of the projectile diameter, $\phi_p = 12.8\ mm$. When the projectile goes through the complete thickness of the plate, the hole starts to decrease due to elastic recovery arising from the rubbery state of amorphous chains within PMMA. Finally, the hole is completely close with some reduced radial cracks.

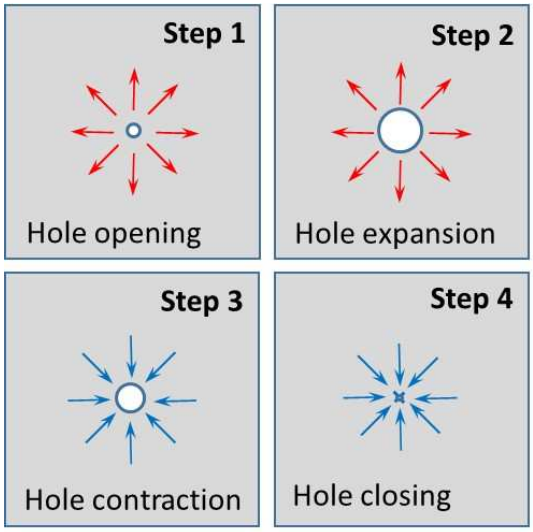

Fig. 6: Kinematics of the failure mode, perforation and structural behaviour of PMMA at high temperature.

4. Modelling of the material yielding at different temperatures using Richeton's model

As a first approach, the Richeton model is used to describe the yielding response of PMMA [17]. This model is frequently reported in the literature to predict the mechanical behaviour of thermoplastic polymers for a large range of temperatures and strain rates [17,25]. The model describes the yield stress value corresponding to the maximum stress level, Figs. 7-8. The model of Richton [17] is based in a previous approach proposed in Ref. [35], where the stress is defined as:

$$\frac{\sigma}{T} = \frac{2k}{V} sinh^{-1}\left(\frac{\dot{\varepsilon}}{\dot{\varepsilon}^*}\right) \tag{3}$$

where k is the Boltzmann constant, V is the activation volume and $\dot{\varepsilon}^*$ is related to the process of thermal activation. Based on the previous expression, a better description of the yield stress is obtained considering the following stress decomposition with the effective yield stress σ^*. Thus, the stress level is defined as:

$$\sigma^* = \sigma - \sigma_i \tag{4}$$

where σ_i is an internal stress associated to the a recovery process. The assumption of this model is that the yield stress is reached when n segments of the amorphous polymer move simultaneously in a cooperative way. The strain rate is then defined as:

$$\dot{\varepsilon} = \dot{\varepsilon}^* sinh^n\left[\frac{(\sigma-\sigma_i)\cdot V}{2kT}\right] \tag{5}$$

Where T is the absolute temperature. Coupling Eqs. (3-5), the following relation is reached:

$$\sigma = \sigma_i + \frac{2kT}{V} sinh^{-1}\left[\left(\frac{\dot{\varepsilon}}{\dot{\varepsilon}^*}\right)^{\frac{1}{n}}\right] \quad (6)$$

To describe the process of thermal activation, $\dot{\varepsilon}^* = \dot{\varepsilon}_0 \, exp\left(\frac{-\Delta H}{kT}\right)$, an Arrhenius equation is used with ΔH_β being an activation energy. As described in Ref. [35], the term σ_i is equal to zero for $T > T_g$. Finally, Richeton et al. [17] added an extra term to increase the temperature sensitivity as:

$$\sigma_Y(\dot{\varepsilon}, T) = \sigma_i(0) - mT + \frac{2kT}{V} sinh^{-1}\left[\frac{\dot{\varepsilon}}{\dot{\varepsilon}_0 \, exp\left(-\frac{\Delta H_\beta}{kT}\right)}\right]^{\frac{1}{n}} \quad \text{for } T \leq T_g \quad (7\text{-a})$$

However, it is observed that the power term $\frac{1}{n}$ is not correctly reported in Eq. 7-a [17] in comparison with the original model proposed in [35]. It induces a decrease of the stress level at low temperatures and at high strain rate sensitivity. The Richeton model is compared with the corrected model reported in this work, Eq. 7-b.

$$\sigma_Y(\dot{\varepsilon}, T) = \sigma_i(0) - mT + \frac{2kT}{V} sinh^{-1}\left[\left(\frac{\dot{\varepsilon}}{\dot{\varepsilon}_0 \, exp\left(-\frac{\Delta H_\beta}{kT}\right)}\right)^{\frac{1}{n}}\right] \quad \text{for } T \leq T_g \quad (7\text{-b})$$

The constants used to describe the material behaviour of PMMA are reported in Table 1.

Table 1: *Constants for PMMA using Eqs. 7a-b and 8a-b.*

Parameters for Eqs. 7a-b	**Material PMMA**	**Units**
$\sigma_i(0)$	190	MPa
m	0.47	MPa/K
k - Boltzmann constant	1.38E-23	$J \cdot K^{-1}$
V	5.14E-29	m^3
$\dot{\varepsilon}_0$	7.46E+15	s^{-1}
ΔH_β	90	$kJ \cdot mol^{-1}$
n	6.37	-
N – Avogadro number	6.022E+23	mol^{-1}
Parameters for Eqs. 8a-b for $T > T_g$	**Material PMMA**	**Units**
T_g	105	$°C$
C_1^g	9	-
C_2^g	35.5	$°C$

It is observed that the original model of Richeton and reported in several works such as Refs. [36,37,38] is not working correctly to describe the material behaviour of PMMA at low temperatures using the previous constants, Table 1 and Eq. 7-a. The lowest limit, as shown in Fig. 7a, is limited to $T = 0°C$. From this value to the glass transition temperature, the two equations Eqs.7-a-b are giving the same trend and similar results. The other problem is observed with the strain rate sensitivity, Fig. 7b. For example, at high temperature and in the range of quasi-static loading, the yield stress values are the same

between Eqs. 7-a. and 7-b. However, under dynamic loading, the models diverge if the strain rate is larger than $\dot{\varepsilon} > 1\ s^{-1}$. However, in his original form it can be assumed a recurrent typo error. Therefore, the model of Richeton has some limitations at low temperatures and high strain rates. Due to this problem and to have a large field of strain rates and temperatures, Eqs. 7-b and 8-b are used.

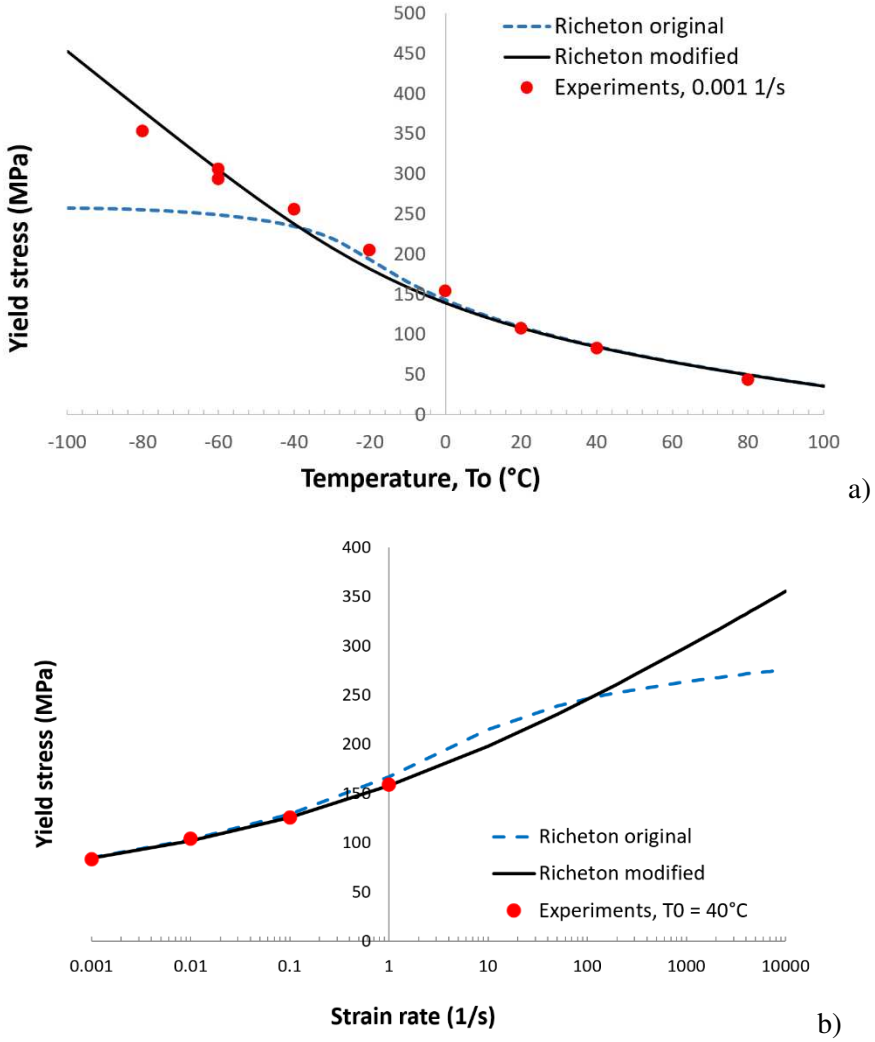

Fig. 7: Comparison between the original Richeton model [17], Eq. 7-a, and the corrected version, Eq. 7-b: a) Temperature sensitivity; b) Strain rate sensitivity at high temperature.

Concerning the behaviour for $T > T_g$, Richeton et al. [17] proposed the expression showed in Eq. 8-a. The same problem as discussed before is that the term $\frac{1}{n}$ is outside of the bracket. To be consistent with the initial description based on the process of thermal activation and assuming a cooperative behaviour, the model must be defined as in Eq. 8-b.

$$\sigma_Y(\dot{\varepsilon},T) = \frac{2kT}{V} sinh^{-1}\left[\frac{\dot{\varepsilon}}{\dot{\varepsilon}_0\, exp\left(-\frac{\Delta H_\beta}{RT}\right)\cdot exp\left(\frac{ln(10)\cdot c_1^g (T-T_g)}{c_2^g + T - T_g}\right)}\right]^{\frac{1}{n}} \quad \text{for} \quad T > T_g \qquad (8\text{-a})$$

$$\sigma_Y(\dot{\varepsilon},T)=\frac{2kT}{V}sinh^{-1}\left(\left[\frac{\dot{\varepsilon}}{\dot{\varepsilon}_0\,exp\left(-\frac{\Delta H_\beta}{RT}\right)\cdot exp\left(\frac{ln(10)\cdot c_1^g(T-T_g)}{c_2^g+T-T_g}\right)}\right]^{\frac{1}{n}}\right) \quad \text{for} \quad T>T_g \qquad (8\text{-b})$$

where $\dot{\varepsilon}_0$ is a constant pre-exponential strain rate and R is the universal gas constant.

However, comparing these two equations, Eq. 8-a and Eq. 8-b, it is observed that the difference is negligible, Fig. 8. Therefore, in this range of temperature, the two equations may be used without large effects. However, to be rigorous and consistent, Eq. 8-b, is used and coupled to Eq. 7-b as previously proposed in Ref. [35].

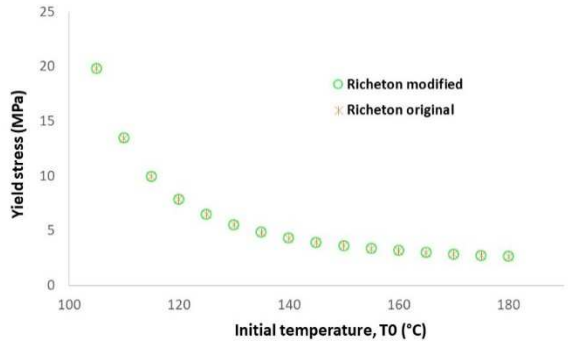

Fig. 8: Comparison between the Richeton model [17], Eq. 8-a, and the corrected version, Eq. 8-b for $T > T_g$.

Some tests have been performed to compare experiments with the Richeton model [17]. It is observed that keeping the same conditions in terms of waiting time and initial temperature, the stress is dispersive. In each case, three to five tests have been performed and the average value is reported, Fig. 9.

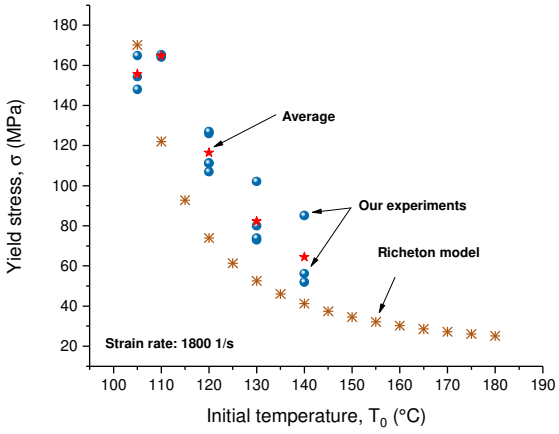

Fig. 9: PMMA material behaviour at high strain rate for different initial temperature.

In the next section, we propose a new constitutive model for finite deformations to further analyse the mechanical transitions at high strain rates and different temperatures.

5. Constitutive model for finite deformations at glass transition

This section analyses the mechanical behaviour of PMMA at high strain rate and temperatures above glass transition. To describe the mechanical behaviour of PMMA at these conditions, we develop here a constitutive model accounting for finite deformations, temperature dependency, adiabatic heating and relaxation-recovery mechanisms.

5.1. Kinematics of the deformation process

The overall mechanical response of the material is understood as the combination of overcoming a purely hyperelastic (Equilibrium) resistance associated to the polymer network, and a visco-hyperelastic (*Non-equilibrium*) resistance associated to relaxation mechanisms and other viscous dependencies. A clear picture of the model is presented in Fig. 10 by means of the equivalent rheological model and the corresponding kinematics scheme. Note that a further decomposition of the mechanical response is done, splitting it into volumetric and isochoric components. To this end, the total deformation gradient $\mathbf{F}$ is broken down into volumetric $\mathbf{F}_{\mathrm{vol}} = J^{1/3}\mathbf{I}$, and isochoric $\mathbf{F}_{\mathrm{iso}} = J^{-1/3}\mathbf{F}$ parts as:

$$\mathbf{F} = \mathbf{F}_{\mathrm{vol}}\mathbf{F}_{\mathrm{iso}} = \mathbf{F}_{\mathrm{e}}\mathbf{F}_{\mathrm{v}} \tag{9}$$

where $J = \det\mathbf{F}$ is the Jacobian and $\mathbf{I}$ is the second-order identity tensor. Note that the isochoric component is further decomposed into elastic $\mathbf{F}_{\mathrm{e}}$ and plastic $\mathbf{F}_{\mathrm{p}}$ components for the *Non-Equilibrium* branch. Therefore, according to Fig. 11-b, Therefore, the deformed configuration Ω can be reached from the reference configuration Ω_{o} by accounting for the total deformation gradient $\mathbf{F}$ or, alternatively, by going through a dilated intermediate configuration $\overline{\Omega}$ by uniquely accounting for the mechanical-induced dilatation. Another intermediate configuration, defined as dilated relaxed configuration $\overline{\overline{\Omega}}$, is defined to help with the formulation of the viscous flow.

To complete the definition of the model kinematics needed to further define the viscous flow rule, the viscous velocity gradient reads as:

$$\mathbf{L}_{\mathrm{v}} = \dot{\mathbf{F}}_{\mathrm{v}}\mathbf{F}_{\mathrm{v}}^{-1} = \mathbf{D}_{\mathrm{v}} + \mathbf{W}_{\mathrm{v}} \tag{10}$$

where $\mathbf{D}_{\mathrm{v}} = \frac{1}{2}\left(\mathbf{L}_{\mathrm{v}} + \mathbf{L}_{\mathrm{v}}^{\mathrm{T}}\right)$ and $\mathbf{W}_{\mathrm{v}} = \frac{1}{2}\left(\mathbf{L}_{\mathrm{v}} - \mathbf{L}_{\mathrm{v}}^{\mathrm{T}}\right)$. The intermediate configuration $\overline{\overline{\Omega}}$ is assumed invariant to rigid body rotations of the current configuration Ω, that is $\mathbf{W}_{\mathrm{v}} = \mathbf{0}$ (Boyce et al., 1988).

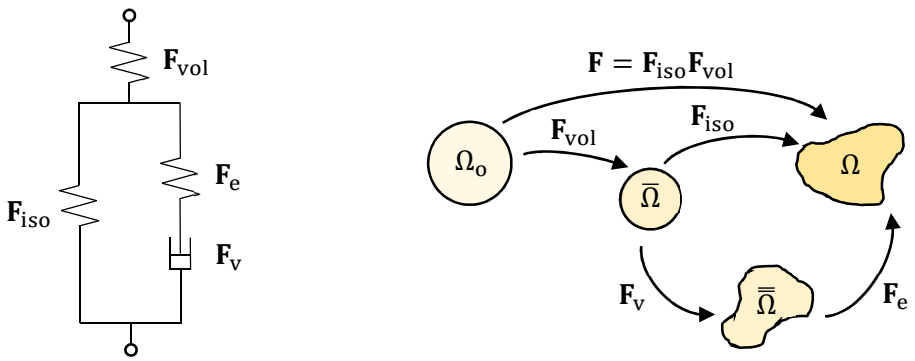

Fig. 10: (a) Rheological model; (b) kinematics scheme of the model.

From the rheological scheme presented and accounting for the corresponding kinematics, the development and specification of the constitutive equations is presented next.

5.2. Constitutive equations

The total Cauchy stress tensor $\boldsymbol{\sigma}$ is defined as the additive contribution of the volumetric $\boldsymbol{\sigma}_{\mathrm{vol}}$, *Equilibrium* $\boldsymbol{\sigma}_{\mathrm{E}}$ and *Non-equilibrium* $\boldsymbol{\sigma}_{\mathrm{Ne}}$ components as:

$$\boldsymbol{\sigma} = \boldsymbol{\sigma}_{\mathrm{vol}} + \boldsymbol{\sigma}_{\mathrm{E}} + \boldsymbol{\sigma}_{\mathrm{Ne}} \tag{11}$$

Volumetric response

The volumetric response is defined by a linear model based on the bulk modulus of the material K as:

$$\boldsymbol{\sigma}_{\mathrm{vol}} = \mathrm{K}(J-1) \tag{12}$$

Equilibrium response

The *Equilibrium* branch represents an entropic resistance associated to the orientation of the molecular chains that constitute the polymer network. A modification of the Arruda-Boyce model [39] is used for this purpose:

$$\boldsymbol{\sigma}_{\mathrm{E}} = \frac{\mu_E}{3J}\frac{\lambda_l}{\bar{\lambda}}\mathcal{L}^{-1}\left(\frac{\bar{\lambda}}{\lambda_l}\right)\left(\mathbf{B}_{iso} - \bar{\lambda}^2\mathbf{I}\right) \tag{13}$$

where μ_E is the *Equilibrium* shear modulus, λ_l is a locking stretch delimiting the maximum extension of the polymer chains, $\bar{\lambda} = \sqrt{\frac{1}{3}tr\left(\mathbf{F}_{iso}\mathbf{F}_{iso}^T\right)}$ is the average stretch and $\mathcal{L}^{-1}$ is the inverse of the Langevin function. Finally, $\mathbf{B}_{iso}$ is the isochoric left Cauchy-Green deformation tensor defined as $\mathbf{B}_{iso} = \mathbf{F}_{iso}\mathbf{F}_{iso}^T$.

Non-equilibrium response

This branch describes the visco-hyperelastic response of the polymer and accounts for strain rate dependency, temperature dependency and relaxation mechanisms. First, the hyperelastic spring is defined following a Neo-Hookean description as [40]:

$$\boldsymbol{\sigma}_{\mathrm{Ne}} = \frac{\mu_{Ne}}{J}\mathbf{B}_e^{dev} \tag{14}$$

where μ_{Ne} is the *Non-equilibrium* shear modulus and $\mathbf{B}_e^{dev}$ is the deviatoric part of the elastic Cauchy-Green deformation tensor defined as $\mathbf{B}_e = \mathbf{F}_e\mathbf{F}_e^T$.

To complete the formulation of the model, the evolution of the viscous deformation gradient must be defined. To this end, the viscous stretch rate $\mathbf{D}_{\mathrm{v}}$ is defined as:

$$\mathbf{D}_{\mathrm{v}} = \frac{\dot{\gamma}_{\mathrm{v}}}{\sqrt{2}\tau_{\mathrm{Ne}}}\boldsymbol{\sigma}_{Ne}^{dev} \tag{15}$$

where $\tau_{\mathrm{Ne}} = \sqrt{tr\left(\boldsymbol{\sigma}_{Ne}^{dev}\boldsymbol{\sigma}_{Ne}^{dev}\right)}$ is the effective stress driving the viscous flow and $\dot{\gamma}_{\mathrm{v}}$ is a visco-elastic multiplier.

A complete definition of the visco-elastic multiplier for the whole temperature regime has been proposed by Richeton et al. [25]. In this work, the authors proposed an expression for the viscous shear strain rate based on a cooperative model originally developed by Povolo and Hermida [35]. In the work of Richeton and coauthors [25], the definition of the viscous multiplier is done by a switching expression from rubbery state (bellow glass transition) to glassy state (above glass transition) as:

$$\dot{\gamma}_{\mathrm{v}} = \begin{cases} \dot{\gamma}_{\mathrm{o}} exp\left(-\frac{\Delta H_{\beta}}{\boldsymbol{RT}}\right) sinh^{n}\left(\frac{(\tau - t_i)V}{2kT}\right), & T < T_g \\ \dot{\gamma}_{\mathrm{o}} exp\left(-\frac{\boldsymbol{\Delta H_{\beta}}}{\boldsymbol{RT}}\right) exp\left(\frac{ln(\mathbf{10})\boldsymbol{c_1^g}(\boldsymbol{T}-\boldsymbol{T_g})}{\boldsymbol{c_2^g}+\boldsymbol{T}-\boldsymbol{T_g}}\right) sinh^{n}\left(\frac{\tau V}{2kT}\right), & T \geq T_g \end{cases} \tag{16}$$

where $\dot{\gamma}_{\mathrm{o}}$ is a pre-exponential shear rate factor, τ is the effective stress and n, t_i, $\boldsymbol{c_1^g}$ and c_2^g are material parameters.

As the propose model is developed to explore the deformation mechanisms of PMMA at high temperatures (above glass transition), we simplified the previous expression for high temperatures as:

$$\dot{\gamma}_{\mathrm{v}} = A\, sinh^{n}\left(\frac{\tau_{\mathrm{Ne}}}{B}\right) \tag{17}$$

where n and B are constant material parameters.

The parameter $A = \hat{A}(T)$ is a temperature-dependent material parameter that introduces yielding dependence on temperature and thermal softening due to adiabatic heating:

$$A = \hat{A}(T) = exp\left(\frac{T - T_g}{m_2}\right)^{m_1} \tag{18}$$

with m_1 and m_2 being temperature sensitivity parameters.

Finally, the temperature evolution due to inelastic dissipation (adiabatic heating) can be derived from thermodynamics principles (see works by Garcia-Gonzalez et al. [27, 16]) as:

$$\bar{C}\dot{T} = \boldsymbol{\sigma}_{Ne}^{dev} : \mathbf{D}_{\mathrm{v}} - \mathrm{Div}\,\mathbf{Q} \tag{19}$$

where $\bar{C}$ is the specific heat, the term $\boldsymbol{\sigma}_{Ne}^{dev}:\mathbf{D}_{\mathrm{v}}$ represents inelastic dissipation and the term $-\mathrm{Div}\,\mathbf{Q}$ represents heat conduction (with $\mathbf{Q}$ being the heat flux per unit area). Note that thermoelastic contributions are neglected here.

5.2. Calibration of the model parameters and discussion

The model parameters have been found using optimization tools in MATLAB based on comparison of model predictions with experimental data for high strain rates and temperatures above glass transition. The final parameters identified are depicted in Table 2. The model predictions are compared to experimental data by means of stress-strain response and yield stress dependency at high temperatures, Fig. 11. A good agreement is found between the model predictions and experiments. Moreover, it is observed that the proposed model captures the temperature dependency of the yield stress, the nonlinear behaviour at large deformations and the thermal softening arising from adiabatic heating.

Table 2. Model parameters for PMMA.

Equilibrium response				
μ_{E} (MPa)	λ_l (-)			
60	1.7			
Non-Equilibrium response				
μ_{Ne} (GPa)	B (MPa)	n (-)	m_1 (-)	m_2 (K)
2.9	50	2.5	0.8	3.5
Physical properties				
T_g (K)	$\bar{C}$ (J/kgK)	ρ (kg/m^3)		
378	1370	1190		

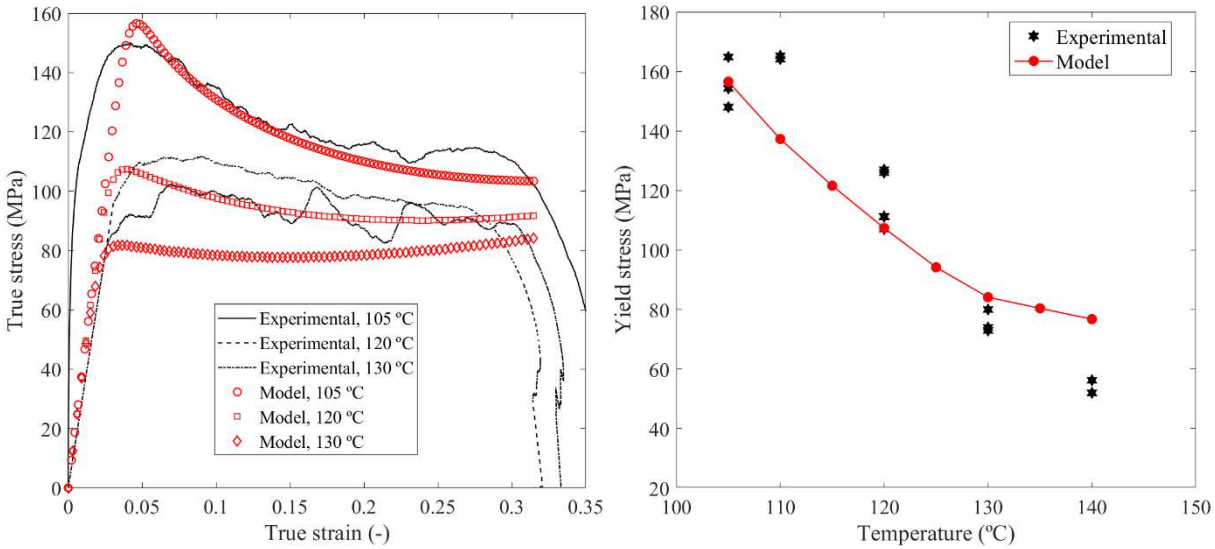

Fig. 11: Comparison between model predictions and experimental data at high strain rates (1500 s^{-1}) and temperatures above glass transition: (left) true stress-true strain curves; (right) yield stress dependence with temperature.

This model permits a theoretical description of experiments evaluating the influence of the polymeric network, viscous mechanisms and hyperelastic-viscous deformations. Thus, increasing the initial temperature testing temperature, the material undergoes lower flow stresses. Moreover, the polymeric network starts to govern the mechanical response leading to higher influence of elastic deformation over plastic contributions, see Fig. 12. These mechanisms explain the stronger softening due to adiabatic heating for lower testing temperatures. In addition, due to governing role of the network contribution at high temperatures and according to the arrangement of the rheological elements (see Fig. 10), relevant spring back effects are expected. Therefore, a transition to rubbery response can explain the experimental observations from impact tests at high temperatures when the material fully recovers closing the hole generated during the perforation process, Figs. 5d and 6.

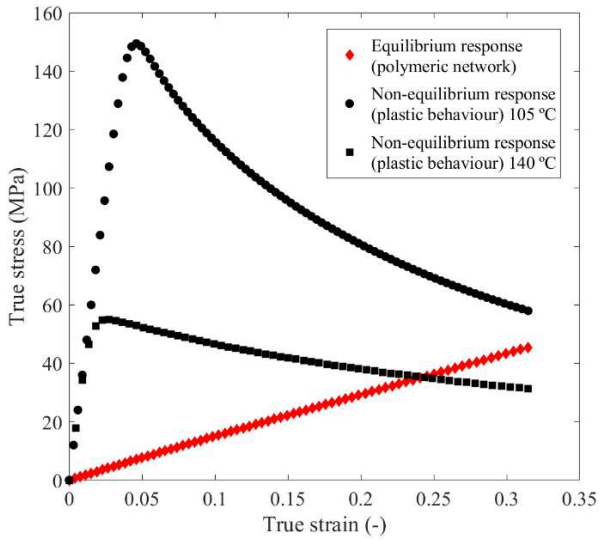

Figure 12: Comparison between polymeric network and plastic contributions for the, according to the proposed model, mechanical behaviour of PMMA at strain rate of 1500 s^{-1} and testing temperatures of 105 ºC (glass transition) and 140 ºC.

Note that the model is limited to high strain rates and temperature avoiding unnecessary extra parameters in the proposed study. However, the model permits extensions to include such dependencies within a thermodynamically consistent framework.

6. Conclusions

This work studies the mechanical behaviour of PMMA under a wide strain rate and temperature conditions, identifying behavioural transitions associated to microstructural changes. To this end, this work presents a complete study of the mechanical response of PMMA at high impact velocity covering testing temperature from 20 ºC to 140 ºC. Before the perforation tests, we performed uniaxial compression tests for both quasi-static and dynamic conditions and different initial temperatures to understand in a better way the deformation and failure mechanisms governing the perforation process. Then, the yielding behaviour of PMMA is analysed revisiting the model developed by Richeton et al. [17]. Finally, a new constitutive model is proposed to analyse the deformation mechanisms governing the mechanical behaviour of PMMA. This model is focused on the mechanical behaviour of PMMA above the glass transition, formulated for finite deformations and accounts for temperature and strain rate dependencies. In addition, the model allows to consider the process of recovering to explain the failure mode observed under dynamic impact and perforation.

Acknowledgments: D. Garcia-Gonzalez acknowledges support from the Talent Attraction grant (CM 2018 - 2018-T2/IND-9992) from the Comunidad de Madrid.

References

[1] Al-Oqla, F. M., & Sapuan, S. M. (2014). Natural fiber reinforced polymer composites in industrial applications: feasibility of date palm fibers for sustainable automotive industry. *Journal of Cleaner Production*, *66*, 347-354.

[2] Biron, M. (2016). *Industrial applications of renewable plastics: environmental, technological, and economic advances*. William Andrew.

[3] Stopp, S., Wolff, T., Irlinger, F., & Lueth, T. (2008). A new method for printer calibration and contour accuracy manufacturing with 3D-print technology. *Rapid Prototyping Journal*, *14*(3), 167-172.

[4] Dudek, P. F. D. M. (2013). FDM 3D printing technology in manufacturing composite elements. *Archives of Metallurgy and Materials*, *58*(4), 1415-1418.

[5] Hopkinson, N., & Dicknes, P. (2003). Analysis of rapid manufacturing—using layer manufacturing processes for production. *Proceedings of the Institution of Mechanical Engineers, Part C: Journal of Mechanical Engineering Science*, *217*(1), 31-39.

[6] Mazurkiewicz, Ł., Małachowski, J., & Baranowski, P. (2015). Optimization of protective panel for critical supporting elements. *Composite Structures*, *134*, 493-505.

[7] Fan, Y., Lu, W. B., Yan, P., Chen, M., & Zhang, Y. Z. (2015). Transient characters of energy changes induced by blasting excavation of deep-buried tunnels. *Tunnelling and Underground Space Technology*, *49*, 9-17.

[8] Pach, J., Pyka, D., Jamroziak, K., & Mayer, P. (2017). The experimental and numerical analysis of the ballistic resistance of polymer composites. *Composites Part B: Engineering*, *113*, 24-30.

[9] Karthick, R., Sirisha, P., & Sankar, M. R. (2014). Mechanical and tribological properties of PMMA-sea shell based biocomposite for dental application. *Procedia materials science*, *6*, 1989-2000.

[10] Koh, Y., Jang, S., Kim, J., Kim, S., Ko, Y. C., Cho, S., & Sohn, H. (2008). DBR PSi/PMMA composite materials for smart patch application. *Colloids and Surfaces A: Physicochemical and Engineering Aspects*, *313*, 328-331.

[11] Rigby, D., & Roe, R. J. (1988). Molecular dynamics simulation of polymer liquid and glass. II. Short range order and orientation correlation. *The Journal of Chemical Physics*, *89*(8), 5280-5290.

[12] Dorogoy, A., & Rittel, D. (2014). Impact of thick PMMA plates by long projectiles at low velocities. Part II: Effect of confinement. *Mechanics of Materials*, *70*, 53-66.

[13] Rittel, D., & Dorogoy, A. (2014). Impact of thick PMMA plates by long projectiles at low velocities. Part I: Effect of head's shape. *Mechanics of Materials*, *70*, 41-52.

[14] Forquin, P., Nasraoui, M., Rusinek, A., & Siad, L. (2012). Experimental study of the confined behaviour of PMMA under quasi-static and dynamic loadings. *International Journal of Impact Engineering*, *40*, 46-57.

[15] Barba, D., Arias, A., & Garcia-Gonzalez, D. (2020). Temperature and strain rate dependences on hardening and softening behaviours in semi-crystalline polymers: Application to PEEK. *International Journal of Solids and Structures*, *182*, 205-217.

[16] Garcia-Gonzalez, D., Garzon-Hernandez, S., & Arias, A. (2018). A new constitutive model for polymeric matrices: Application to biomedical materials. *Composites Part B: Engineering*, *139*, 117-129.

[17] Richeton, J., Ahzi, S., Vecchio, K. S., Jiang, F. C., & Adharapurapu, R. R. (2006). Influence of temperature and strain rate on the mechanical behavior of three amorphous polymers: Characterization and modeling of the compressive yield stress. *International journal of solids and structures*, *43*(7-8), 2318-2335.

[18] Mulliken, A. D., & Boyce, M. C. (2006). Mechanics of the rate-dependent elastic–plastic deformation of glassy polymers from low to high strain rates. *International journal of solids and structures*, *43*(5), 1331-1356.

[19] Rusinek, A., Bernier, R., Boumbimba, R. M., Klosak, M., Jankowiak, T., & Voyiadjis, G. Z. (2018). New devices to capture the temperature effect under dynamic compression and impact perforation of polymers, application to PMMA. *Polymer Testing*, *65*, 1-9.

[20] Frick, B., Richter, D., & Ritter, C. (1989). Structural changes near the glass transition–neutron diffraction on a simple polymer. *EPL (Europhysics Letters)*, *9*(6), 557.

[21] Garcia-Gonzalez, D., Rodriguez-Millan, M., Rusinek, A., & Arias, A. (2015). Investigation of mechanical impact behavior of short carbon-fiber-reinforced PEEK composites. *Composite Structures*, *133*, 1116-1126.

[22] Garcia-Gonzalez, D., Rusinek, A., Jankowiak, T., & Arias, A. (2015). Mechanical impact behavior of polyether–ether–ketone (PEEK). *Composite Structures*, *124*, 88-99.

[23] Mohagheghian, I., McShane, G. J., & Stronge, W. J. (2015). Impact perforation of monolithic polyethylene plates: Projectile nose shape dependence. *International Journal of impact engineering*, *80*, 162-176.

[24] Garcia-Gonzalez, D., Rodriguez-Millan, M., Rusinek, A., & Arias, A. (2015). Low temperature effect on impact energy absorption capability of PEEK composites. *Composite Structures*, *134*, 440-449.

[25] Richeton, J., Ahzi, S., Vecchio, K. S., Jiang, F. C., & Makradi, A. (2007). Modeling and validation of the large deformation inelastic response of amorphous polymers over a wide range of temperatures and strain rates. *International journal of solids and structures*, *44*(24), 7938-7954.

[26] Boyce, M. C. (1996). Direct comparison of the Gent and the Arruda-Boyce constitutive models of rubber elasticity. *Rubber chemistry and technology*, *69*(5), 781-785.

[27] Garcia-Gonzalez, D., Zaera, R., & Arias, A. (2017). A hyperelastic-thermoviscoplastic constitutive model for semi-crystalline polymers: application to PEEK under dynamic loading conditions. *International Journal of Plasticity*, *88*, 27-52.

[28] Lennon, A. M., & Ramesh, K. T. (1998). A technique for measuring the dynamic behavior of materials at high temperatures. *International Journal of Plasticity*, *14*(12), 1279-1292.

[29] Wang, K., Bahlouli, N., Boumbimba, R. M., Addiego, F., & Rémond, Y. (2016). Specimen geometry effect on the deformation mechanisms of polypropylene-based composites under impact loading at different temperatures. *Journal of Dynamic Behavior of Materials*, *2*(1), 101-111.

[30] Klosak, M., Rusinek, A., Jankowiak, T., El Qoubba, Z., Boumbimba, R. M., & Bendarma, A. (2018). Dynamic perforation and compression tests of PMMA for a wide range of temperatures-experimental and preliminary numerical analysis. In *EPJ Web of Conferences* (Vol. 183, p. 02055). EDP Sciences.

[31] Jankowiak, T., Rusinek, A., & Bendarma, A. (2018). Protocol to define material behaviour and failure strain level at low and high strain rates based on compression test. *Journal of Theoretical and Applied Mechanics*, *56*(2), 471-481.

[32] Bendarma, A., Jankowiak, T., Rusinek, A., Lodygowski, T., & Klosak, M. (2019, March). Perforation Tests of Aluminum Alloy Specimens for a Wide Range of Temperatures Using High-Performance Thermal Chamber-Experimental and Numerical Analysis. In *IOP Conference Series: Materials Science and Engineering* (Vol. 491, No. 1, p. 012027). IOP Publishing.

[33] Jia, B., Rusinek, A., Bahi, S., Bernier, R., Pesci, R., & Bendarma, A. (2019). Perforation Behavior of 304 Stainless Steel Plates at Various Temperatures. *Journal of Dynamic Behavior of Materials*, *5*(4), 416-431.

[34] Recht, R., & Ipson, T. W. (1963). Ballistic perforation dynamics. *Journal of Applied Mechanics*, *30*(3), 384-390.

[35] Povolo, F., & Hermida, É. B. (1995). Phenomenological description of strain rate and temperature-dependent yield stress of PMMA. *Journal of Applied Polymer Science*, *58*(1), 55-68.

[36] Srivastava, V., Chester, S. A., Ames, N. M., & Anand, L. (2010). A thermo-mechanically-coupled large-deformation theory for amorphous polymers in a temperature range which spans their glass transition. *International Journal of Plasticity*, *26*(8), 1138-1182.

[37] Nasraoui, M., Forquin, P., Siad, L., & Rusinek, A. (2012). Influence of strain rate, temperature and adiabatic heating on the mechanical behaviour of poly-methyl-methacrylate: experimental and modelling analyses. *Materials & Design*, *37*, 500-509.

[38] Liu, W., Gao, Z., & Yue, Z. (2008). Steady ratcheting strains accumulation in varying temperature fatigue tests of PMMA. *Materials Science and Engineering: A*, *492*(1-2), 102-109.

[39] Arruda, E. M., & Boyce, M. C. (1993). Evolution of plastic anisotropy in amorphous polymers during finite straining. *International Journal of Plasticity*, *9*(6), 697-720.

[40] Rivlin, R. S. (1948). Large elastic deformations of isotropic materials IV. Further developments of the general theory. *Philosophical Transactions of the Royal Society of London. Series A, Mathematical and Physical Sciences*, *241*(835), 379-397.